Article

Single Gold-Nanoparticle-Enhanced Raman Scattering of Individual Single-Walled Carbon Nanotubes via Atomic Force Microscope Manipulation

Lianming Tong, Zhipeng Li, Tao Zhu, Hongxing Xu, and Zhongfan Liu

More About This Article

Additional resources and features associated with this article are available within the HTML version:

- Supporting Information
- Links to the 2 articles that cite this article, as of the time of this article download
- Access to high resolution figures
- Links to articles and content related to this article
- Copyright permission to reproduce figures and/or text from this article

View the Full Text HTML

Single Gold-Nanoparticle-Enhanced Raman Scattering of Individual Single-Walled Carbon Nanotubes via Atomic Force Microscope Manipulation

Lianming Tong,[†] Zhipeng Li,[‡] Tao Zhu,*,[†] Hongxing Xu,*,[‡,§] and Zhongfan Liu*,[†]

Center for Nanoscale Science and Technology, Beijing National Laboratory for Molecular Sciences, State Key Laboratory for Structural Chemistry of Unstable and Stable Species, College of Chemistry and Molecular Engineering, Peking University, Beijing, 100871, People's Republic of China, State Key Laboratory for Surface Physics, Institute of Physics, Chinese Academy of Sciences, Beijing, 100080, People's Republic of China, and Division of Solid State Physics, Department of Physics, Lund University, Box 118, SE-22100, Lund, Sweden

Investigating the electric field distribution around individual metallic nanoparticles is of significant importance for the understanding of the electromagnetic (EM) mechanism of surface-enhanced Raman scattering (SERS). We report single gold-nanoparticle-enhanced Raman scattering of individual single-walled carbon nanotubes (SWNTs) by atomic force microscope (AFM) manipulation. The distance between the gold nanoparticle (GNP) and the SWNT can be controlled by pushing the GNP with an AFM tip. The Raman signals increase when a single GNP is moved close to an individual SWNT, and the corresponding polarization dependence to the incident laser excitation at each GNP/SWNT distance is studied. The agreement of the experimental results with the theoretical model described in this paper suggests a rational modification of the EM enhancement model of SERS for one-dimensional "molecules", like nanotubes.

Introduction

Surface-enhanced Raman scattering (SERS) has been a significant issue in the research of optical properties of metallic nanostructures and chemo/bio-sensing.[1−4] The huge electric field enhancement, which is induced by surface plasmon resonance (SPR), results in a magnified Raman scattering signal.[5−7] The distribution of the induced electric field around metallic nanostructures has been extensively studied, such as the size and shape effect,[4,8] and distance dependence.[9−14] To further clarify the electromagnetic (EM) mechanism, SERS has been achieved on substrates varying from large metallic nanostructure arrays to individual metallic nanoparticles, so that it is possible to investigate the EM mechanism at single particle level.[6,15,16]

Single-walled carbon nanotubes (SWNTs) have attracted intense scientific interests recently because of their unique electrical, mechanical and optical properties,[17−20] and large potentials in various applications.[21] Spectral measurements, such as fluorescence,[19,22] Raman scattering[23] and Rayleigh scattering,[20,24] are effective means to characterize the vibrational and/or electronic properties of SWNTs. Among these, Raman scattering is a useful tool to study both vibrational and electronic information of SWNTs even down to individual SWNTs level.[23,25]

Because of the high aspect ratio, stability and strong electron−phonon coupling, SWNTs are unique probing molecules for SERS studies.[26,27] On the other hand, SERS can also provide even more detailed structural information of individual SWNTs.[26,28] Tip-enhanced near-field Raman spectroscopy of individual SWNT or SWNT bundle has been reported.[29−32] The high resolution of the metallic tip makes it possible to optically study the inhomogeneous physical or chemical properties, such as chirality and defects, along the SWNT axis with a spatial resolution of tens of nanometers. What is more, the SWNT/tip distance dependence of Raman enhancement has also been studied.[29] Herein, we experiment with SERS of individual SWNTs using single gold nanoparticles (GNPs) as the source of the enhancement manipulated by an atomic force microscope (AFM). The distance between a GNP and an individual SWNT was adjusted by moving the GNP with an AFM tip.

Experimental Methods

Well-separated long SWNTs on SiO_2 substrate were grown by catalytic chemical vapor deposition (CVD).[33,34] Trenches and crosses at micron scale were previously fabricated on the substrate by photolithography and used as markers to locate individual SWNTs. GNPs of ∼12 nm diameter were prepared by sodium citrate reduction of hydrogen tetrachloroaurate (III) trihydrate ($HAuCl_4 \cdot 3H_2O$) and were then used as seeds for synthesizing larger ones.[35]

The sample with SWNTs was then immersed into the Au hydrosol, followed by rinsing with ultrapure water (18.2 MΩ cm) and drying with highly purified nitrogen. The immersion time was determined by the expected surface distribution of GNPs on the substrate. With the prefabricated markers on the substrate, the same SWNTs and GNPs, before and after the AFM manipulations, were easily located under AFM and the objective of the micro-Raman spectroscope.

Raman spectra of SWNTs were measured using a Renishaw system 1000 micro-Raman spectrometer equipped with a He−Ne laser (632.8 nm) and an Olympus microscope (50× objective, numerical aperture: 0.80). The exposure time for a single spectrum was 10 s, and the laser power on the sample for all the measurements was 1 mW. The incident polarization was altered by rotating a half-wave plate inserted before the microscope objective. Such a configuration avoids the effects

* Corresponding authors. E-mail: (T. Z.) zhutao@pku.edu.cn; (H.X.) hxxu@aphy.iphy.ac.cn; (Z.L.) zfliu@pku.edu.cn.
† Peking University.
‡ Chinese Academy of Sciences.
§ Lund University.

of the polarization-dependent sensitivity of the spectrometer grating.[36,37] The Raman scattering signals were collected without any analyzer polarizer. The maximum Raman intensities in the same area before and after the manipulation of GNP can be obtained from Raman spectral mapping. AFM manipulations of GNPs were done on a Nanoscope III SPM (Veeco) equipped with a homemade software.[38] All measurements were done at room temperature. After each manipulation, the sample was baked in air at 300 °C for 5 min to clean the possible contamination on the surface of GNP introduced by the AFM tip. For the SWNTs, Raman spectra show that there is no observable damage caused by laser irradiation or the bake process (see Supporting Information).

Results and Discussion

Raman spectra of SWNTs are generally dominated by two bands, that is, the radial breathing mode (RBM) and the tangential (G) mode.[23,39] RBM is relevant to the coherent vibration of C atoms in the radial direction and occurs between 120 and 350 cm^{-1} for SWNTs of diameters from 0.7 to 2 nm.[23] The frequency of G band varies from 1550 to 1610 cm^{-1}, depending on the chirality and diameter of SWNTs. G$^+$ band, the higher frequency component, is associated with vibrations along the axis of the SWNT, and G$^-$ band, the lower frequency component, is associated with vibrations along the circumferential direction.[23]

The experimental scheme is shown in Figure 1a. The Raman signal was collected in back-scattering direction. Figure 1b,c shows typical Raman mapping images (G$^+$ band) of two sections of a long SWNT without and with a GNP nearby. As shown in Figure 1b, for the section without a GNP, the Raman intensity of the G$^+$ band was homogeneous along the tube axis. However, a sharp contrast in the Raman intensity appeared where there was a GNP nearby, as shown in Figure 1c, which suggests that the Raman scattering of the SWNT can be locally enhanced by the GNP. Figure 1d shows typical Raman spectra of this individual SWNT captured from the points close to and away from the GNP. The Raman intensity of the G$^+$ band at the point close to the GNP was enhanced about three times. In addition, the RBM peak appeared in the GNP enhanced spectrum, while it was merged into the background of the spectrum without GNPs, as shown by the inset in Figure 1d.

On a selected region, the relative positions of the SWNT and GNPs can be further adjusted by AFM manipulation. Figure 2a I−III shows AFM images of a selected region where a GNP of 110 nm diameter (marked by the circle) was pushed away from and close to a long SWNT. The distances from the manipulated GNP to the SWNT in image II and III were estimated to be ∼10 and ∼30 nm (see below), respectively. The corresponding Raman spectra are shown in Figure 2b. It is apparent that the Raman intensity increased dramatically when the GNP was moved closer to the SWNT (Figure 2a, image II), while a decrease occurred when the GNP was slightly pushed away (Figure 2a, image III).

Before the manipulation, only one weak peak at 127 cm^{-1} was observed in the RBM region of the Raman spectrum, as shown in Figure 2b. According to the empirical equation $d_t \sim 248/\omega$ for individual SWNTs on SiO$_2$ surface,[25] where d_t (nm) is the diameter of SWNTs, ω (cm^{-1}) is the frequency of RBM mode and the parameter 248 has a unit of cm^{-1}nm, the estimated diameter of this SWNT is ∼1.9 nm, which is much smaller than the height measured by AFM (4.2 ± 0.5 nm). It indicates that the observed SWNT must be a bundle of several nanotubes with only one in good enough resonant condition to be observed
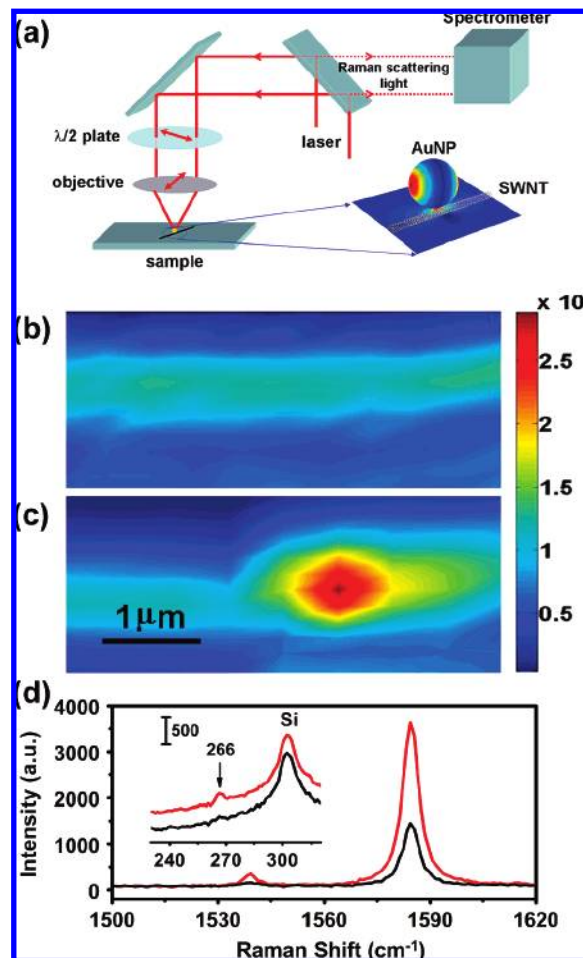
Figure 1. Schematic view of the experimental setup and Raman spectra of an individual SWNT with and without GNPs. (a) Schematic view of the experimental setup. (b,c) Raman mapping (G$^+$ band) images of an individual SWNT without GNPs and with a GNP as the source of the enhancement. (d) The corresponding Raman spectra (black and red curves: the intense region in panels b and c, respectively). Inset, RBM band at 266 cm^{-1}.

in Raman spectra. After being enhanced by the GNP, a weak peak at 173 cm^{-1} appeared, as shown in Figure 2b, suggesting that another SWNT with the estimated diameter of 1.4 nm ($d_t \sim 248/\omega$) must exist in this bundle (also see Supporting Information). It is worthy to point out that resonance Raman spectroscopic characterization of an isolated SWNT sample may not provide enough spectral details to recognize whether it is a single nanotube or a small bundle, because some SWNTs out of resonance may be "invisible" in normal Raman spectra under a certain excitation wavelength.[25] Therefore, SERS spectra of SWNTs provide a possible way to solve the above-mentioned problem to a certain extent, that is, distinguishing SWNT bundles from individual SWNTs. In addition, some weak Raman active modes, such as the intermediate frequency modes,[40] of an individual single SWNT could be clearly seen in the SERS spectra (data not shown here) although not in resonance Raman spectra.

The observed Raman enhancement was caused by the induced electric field of the GNP acting on the SWNT when the GNP was moved closer. Figure 2c shows the electric field profile of a 110 nm spherical GNP on SiO$_2$ substrate, simulated by generalized Mie theory with considering the substrate effect.[41] The dotted lines represent the position of the SWNTs with D denoting the distance between the GNP and the SWNT. It is

Single GNP SERS of Individual SWNTs via AFM Manipulation

J. Phys. Chem. C, Vol. 112, No. 18, 2008 **7121**
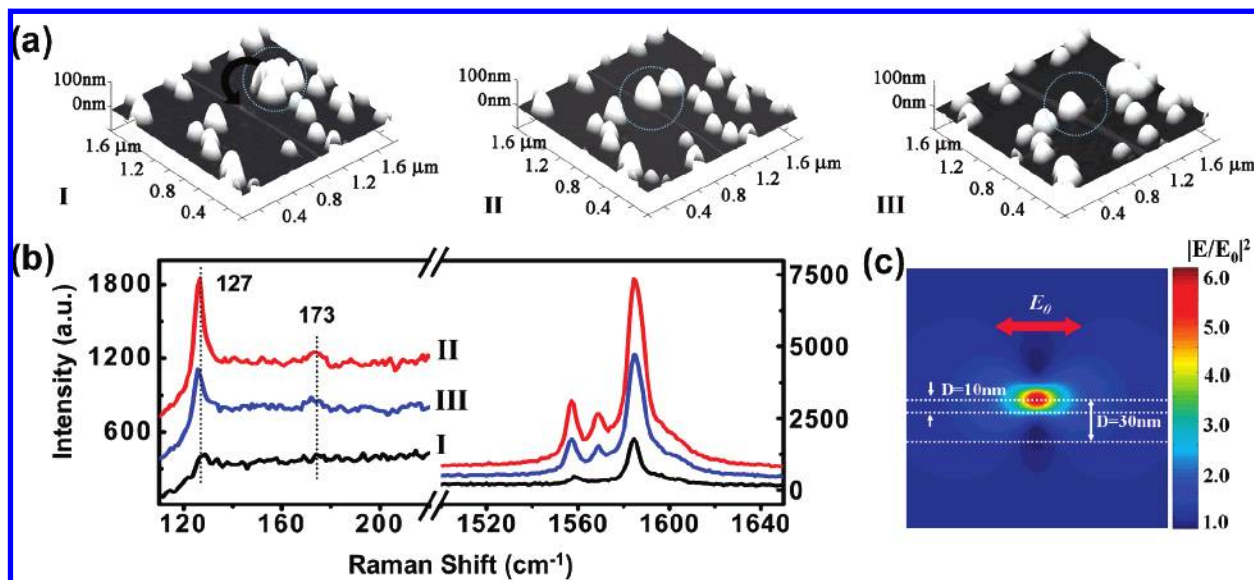
Figure 2. AFM images of a manipulated GNP and the corresponding Raman spectra. (a) AFM images (1.8 μm $\times$ 1.8 μm) of a single GNP and a SWNT at distances D of $\sim$200 (I), $\sim$10 (II) and $\sim$30 nm (III), respectively. (b) The corresponding Raman spectra for I (black), III (blue), and II (red) in panel a. (c) The electric field profile on the substrate under the GNP simulated by the generalized Mie theory. The laser polarization is parallel to the axis of the SWNT.
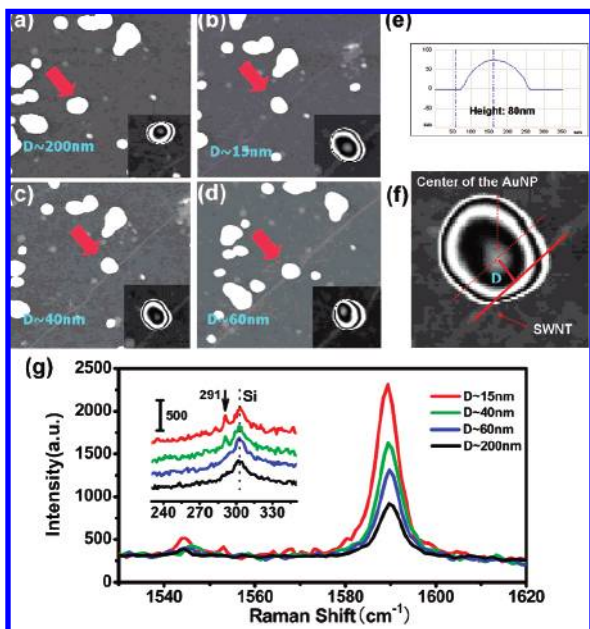
Figure 3. AFM images and single-GNP-enhanced Raman spectra of an individual SWNT at different distance D. (a−d) AFM images (1.8 μm $\times$ 1.8 μm) of the SWNT and GNP. The distance D is $\sim$200 nm for (a), $\sim$15 nm for (b), $\sim$40 nm for (c), and $\sim$60 nm for (d). Insets in panels a−d show the magnified contour images to clarify the relative position of the GNP and the SWNT. (e) The section profile of the GNP indicated by the arrow. (f) The estimation of the distance between the center of the GNP's projection and the SWNT in the contour image (see Supporting Information for details). (g) The corresponding Raman spectra (black for (a), red for (b), green for (c), and blue for (d)). Inset, the RBM region. The polarization of the incident laser is parallel to the axis of the SWNT.

clear that the smaller the distance is, the more intense the electric field the SWNT experiences.

Figure 3a shows the AFM image (1.8 $\times$ 1.8 μm) of a section of a long individual SWNT before the GNP was pushed closer by AFM manipulation. The original distance between the center of the GNP's projection (80 nm diameter, marked by the arrow) and the SWNT was $\sim$200 nm. The induced EM field of the

GNP at such a distance could be attenuated to such a low level that the measured Raman intensity of the SWNT, in this case, was similar to that of the SWNT without any GNPs nearby (see Supporting Information), which can be taken as the basis for comparison. Figure 3b−d shows the AFM images of the same region after AFM manipulation, in which the measured distance (D) between the GNP and the SWNT were $\sim$15, $\sim$40, and $\sim$60 nm, respectively. The scheme for estimating the distance between the GNP and the SWNT is shown in Figure 3f and described in detail in Supporting Information.

Figure 3g shows Raman spectra that were taken from the same region corresponding to the above images with the incident polarization parallel to the SWNT axis. The intensities of the G$^+$ band and RBM peak (inset) are the strongest at a distance of $\sim$15 nm and decrease with the increased distances, as the peak positions remain unchanged. Because there were three other nearby GNPs that were close to the SWNT in Figure 3d, we carefully compared the Raman spectra of the section of SWNT in Figure 3a ($D \sim$ 200 nm) before and after the nearby GNPs being pushed away and the section without GNPs of the same SWNT in other areas. No discrepancies in both intensity and peak position were observed, which indicates that the Raman enhancement was only caused by the manipulated GNP of 80 nm in diameter (see Supporting Information).

The observed SWNT in this region was confirmed to be an individual single SWNT by the consistency between the estimated diameter of the SWNT from RBM frequency at 291 cm^{-1} ($d_t \sim 248/\omega = 0.85$ nm) and the AFM measured height of the SWNT (0.9 ± 0.2 nm). It should also be noted that the RBM peak is "invisible" without SERS enhancement.

At each distance, the Raman spectra at different polarization angles were measured as well, as shown in Figure 4a. The polarization dependence for the GNP at 200 nm distance shows a clear $\cos^2 \theta$ dependency, which is the same as that in normal Raman measurement.[36] At such a distance, no obvious SERS effect can be observed. When the GNP was moved closer, the Raman intensity was enhanced notably in all polarization angles. However, the $\cos^2 \theta$ dependency was obviously broken here becasue there was nonzero minimum Raman intensity at the perpendicular polarization,[42] while $\cos^2 \theta$ predicts a zero value.
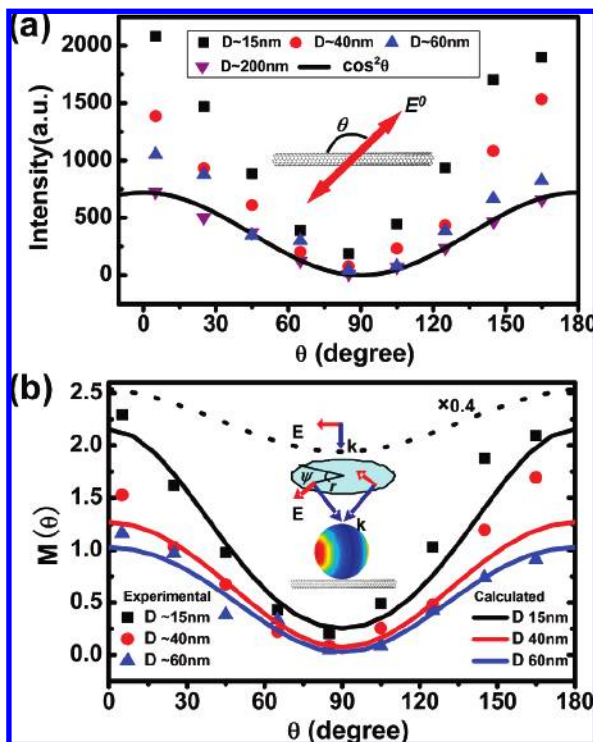
Figure 4. Polarization dependence of G$^+$ band intensity at different distance D and experimental and theoretical Raman enhancement. (a) Raman intensity of G$^+$ band as a function of the polarization angle θ for D at ~200 nm (purple), ~60 nm (blue), ~40 nm (red), and ~15 nm (black), respectively. The purple triangles are fitted by cos$^2\theta$ (black curve). Inset, the definition of polarization angle θ. (b) The experimental EF (markers) and theoretical Raman enhancement (curves) for D at 15 nm (black), 40 nm (red), and 60 nm (blue), respectively. Inset, scheme for the calculation. E and $\boldsymbol{k}$ denote the directions of the polarization and wave vector of the incident light and convergent light from one part of the objective. The dashed curve represents the simulated result by considering the total E_{loc} instead of E_x at the distance of 15 nm for comparison.

It can be explained by an enhanced nonzero electric field parallel to the SWNT, which was induced by the GNP. The antenna effect of the GNP will cause additional Raman enhancement of the SWNT. To simulate the experimental results, we calculated the EM enhancement using the generalized Mie theory with considering the configuration of light focusing and the substrate effect. The substrate effect is accounted as the interaction between the particle and its mirror image inside the substrate.[41] The light at the focus is assumed to be the sum of a number of plane waves that come from every part of the objective. The vector and polarization of these waves are determined by the geometrical optics. Under this least approximation, the expressions of the average electric-field intensity are

$$\bar{E}_i^2(l, \theta) = \frac{1}{\pi r^2} \int_0^{2\pi} \int_0^r E_i^2(r, \varphi, l, \theta) r \, dr \, d\varphi$$

$$i = x, y, z$$

where r and φ are radial and angular coordinates of a point on the objective (see the inset of Figure 4b), and E_i is the electric field calculated by the generalized Mie theory including the substrate-particle coupling.

For SWNTs near the nanoparticle, the enhanced near-field has a component parallel to the SWNT whatever the incident polarization is. The perpendicular components are ignored as only the parallel component of the incident electric field can

excite the Raman scattering process of the SWNT efficiently.[36] The distance between the SWNT and GNP is relatively large (≥ 15 nm), which means the symmetry-lowering effects mentioned by Kneipp et al.[43] should be unlikely accounted here. Hence, the calculated enhancement factor is written as

$$\bar{M}(\theta) = \int_0^L \frac{1}{L} \left| \frac{\bar{E}_x}{E_0} \right|^2 \cdot \left| \frac{\bar{E}}{E_0} \right|^2 dl$$

where L is the length of the SWNT that experienced the induced electric field, which is taken as the diffraction limit of the focused laser beam (~300 nm). E_0 is the electric field of the incident light.

In Figure 4b, the dots and curves represent the experimental enhancement factor (EF) values and theoretical Raman enhancement for D at 15, 40, and 60 nm, respectively. The experimental EF here is defined as the ratio of the enhanced Raman scattering intensity of G$^+$ band to the original intensity under a parallel polarization configuration without GNPs. Obviously, the observed single-GNP SERS polarization dependence of individual SWNT can be appropriately explained by the pure EM simulation. It should be noted that at the distances used here, the single SWNT may have no contact with the GNP if the shape of the GNP is spherical (see Supporting Information). Hence, the chemical enhancement that requires chemisorption of the probe molecules will be ruled out in such a single-nanoparticle/single-nanotube system.

Interestingly, the theoretical method presented here is different from the traditional SERS theory. In the traditional SERS theory, the EF is roughly proportional to the product of the enhancement of the local field which the molecule experiences and the emission enhancement in the Raman channel due to the antenna effect of the surrounding metallic nanostructures, which can be expressed as $M(\theta) \approx |E_{loc}(\omega)/E_0(\omega)|^2 \cdot |(E_{loc}(\omega - \omega_v))/(E_0(\omega - \omega_v))|^2$, where E_0 and E_{loc} are the incident and induced electric filed, and ω and ω_v are the incident frequency and the vibrational frequency of the test molecule, respectively. For SWNTs, the Raman scattering shows a clear cos$^2 \theta$ incident polarization dependency, which means that only the electric field aligned to the direction of the nanotube can cause strong enough Raman scattering. Hence the field enhancement term is changed to $|E_x(\omega)/E_0(\omega)|^2$ for single SWNT instead, where E_x is the induced electric field aligned to the axis of the nanotube. Since E_x is only a partial component of E_{loc}, the contributions to the SERS EF are significantly different. The dashed curve in Figure 4b represents the simulated result by considering the total E_{loc} instead of E_x at a distance of 15 nm. It is obvious that neither the absolute enhancement nor the polarization dependence is in accordance with the experimental values. Hence, the agreement of the experiments and the modified EM model described here suggests a rational modification of the EM model for the EM enhancement mechanism of SERS for one-dimensional "molecules", like SWNTs.

Conclusion

We use AFM manipulated single GNP to obtain SERS spectra from individual SWNT(s). The measured Raman enhancement strongly depends on the distance between the single nanoparticle and the individual SWNT, which can be modulated by AFM manipulation, and significantly depends on the polarization angles. At the large enough distances, the chemical enhancement that requires chemisorption can be ruled out in such a single-particle/single-nanotube system. The agreement between the experimental results and the theoretical model is achieved, which

suggests a rational modification to the EM enhancement of the normal SERS theory for one-dimensional Raman active molecules, such as SWNTs. On the other hand, the enhanced Raman spectra may provide a possible way to distinguish SWNT bundles from individual SWNTs. Also, GNPs of different size, number and morphology can be selectively manipulated to enhance the Raman scattering of the SWNT, which makes it a feasible way to study the electric field distribution around different GNPs (or other metallic nanoparticles, for example, Ag nanoparticles) at individual nanoparticle level.

Supporting Information Available: Additional information available as noted in text. This material is available free of charge via the Internet at http://pubs.acs.org.

References and Notes

(1) Kneipp, K.; Kneipp, H.; Itzkan, I.; Dasari, R. R.; Feld, M. S. *Chem. Rev.* **1999**, *99*, 2957.
(2) Kneipp, K.; Kneipp, H.; Kneipp, J. *Acc. Chem. Res.* **2006**, *39*, 443.
(3) Schatz, G. C.; Young, M. A.; VanDuyne, R. P. *Top. Appl. Phys.* **2006**, *103*, 19.
(4) Haes, A. J.; Haynes, C. L.; McFarland, A. D.; Schatz, G. C.; Van Duyne, R. R.; Zou, S. L. *MRS Bull.* **2005**, *30*, 368.
(5) Kneipp, K.; Wang, Y.; Kneipp, H.; Perelman, L. T.; Itzkan, I.; Dasari, R.; Feld, M. S. *Phys. Rev. Lett.* **1997**, *78*, 1667.
(6) Nie, S. M.; Emery, S. R. *Science* **1997**, *275*, 1102.
(7) Xu, H. X.; Bjerneld, E. J.; Kall, M.; Borjesson, L. *Phys. Rev. Lett.* **1999**, *83*, 4357.
(8) Xu, H. X.; Aizpurua, J.; Kall, M.; Apell, P. *Phys. Rev. E* **2000**, *62*, 4318.
(9) Rechberger, W.; Hohenau, A.; Leitner, A.; Krenn, J. R.; Lamprecht, B.; Aussenegg, F. R. *Opt. Commun.* **2003**, *220*, 137.
(10) Su, K. H.; Wei, Q. H.; Zhang, X.; Mock, J. J.; Smith, D. R.; Schultz, S. *Nano Lett.* **2003**, *3*, 1087.
(11) Gunnarsson, L.; Rindzevicius, T.; Prikulis, J.; Kasemo, B.; Kall, M.; Zou, S. L.; Schatz, G. C. *J. Phys. Chem. B* **2005**, *109*, 1079.
(12) Kelly, K. L.; Coronado, E.; Zhao, L. L.; Schatz, G. C. *J. Phys. Chem. B* **2003**, *107*, 668.
(13) Jain, P. K.; Huang, W. Y.; El-Sayed, M. A. *Nano Lett.* **2007**, *7*, 2080.
(14) Xu, H. X.; Kall, M. *Top. Appl. Phys.* **2006**, *103*, 87.
(15) Imura, K.; Okamoto, H.; Hossain, M. K.; Kitajima, M. *Nano Lett.* **2006**, *6*, 2173.
(16) Svedberg, F.; Li, Z. P.; Xu, H. X.; Kall, M. *Nano Lett.* **2006**, *6*, 2639.
(17) Morpurgo, A. F.; Kong, J.; Marcus, C. M.; Dai, H. *Science* **1999**, *286*, 263.
(18) Li, F.; Cheng, H. M.; Bai, S.; Su, G.; Dresselhaus, M. S. *Appl. Phys. Lett.* **2000**, *77*, 3161.
(19) Lefebvre, J.; Homma, Y.; Finnie, P. *Phys. Rev. Lett.* **2003**, *90*, 217401.
(20) Sfeir, M. Y.; Beetz, T.; Wang, F.; Huang, L. M.; Huang, X. M. H.; Huang, M. Y.; Hone, J.; O'Brien, S.; Misewich, J. A.; Heinz, T. F.; Wu, L. J.; Zhu, Y. M.; Brus, L. E. *Science* **2006**, *312*, 554.
(21) Baughman, R. H.; Zakhidov, A. A.; de Heer, W. A. *Science* **2002**, *297*, 787.
(22) O'Connell, M. J.; Bachilo, S. M.; Huffman, C. B.; Moore, V. C.; Strano, M. S.; Haroz, E. H.; Rialon, K. L.; Boul, P. J.; Noon, W. H.; Kittrell, C.; Ma, J. P.; Hauge, R. H.; Weisman, R. B.; Smalley, R. E. *Science* **2002**, *297*, 593.
(23) Dresselhaus, M. S.; Dresselhaus, G.; Saito, R.; Jorio, A. *Phys. Rep.* **2005**, *409*, 47.
(24) Sfeir, M. Y.; Wang, F.; Huang, L. M.; Chuang, C. C.; Hone, J.; O'Brien, S. P.; Heinz, T. F.; Brus, L. E. *Science* **2004**, *306*, 1540.
(25) Jorio, A.; Saito, R.; Hafner, J. H.; Lieber, C. M.; Hunter, M.; McClure, T.; Dresselhaus, G.; Dresselhaus, M. S. *Phys. Rev. Lett.* **2001**, *86*, 1118.
(26) Kneipp, K.; Kneipp, H.; Dresselhaus, M. S.; Lefrant, S. *Philos. Trans. Roy. Soc. London, Ser. A* **2004**, *362*, 2361.
(27) Kneipp, K.; Kneipp, H.; Corio, P.; Brown, S. D. M.; Shafer, K.; Motz, J.; Perelman, L. T.; Hanlon, E. B.; Marucci, A.; Dresselhaus, G.; Dresselhaus, M. S. *Phys. Rev. Lett.* **2000**, *84*, 3470.
(28) Duesberg, G. S.; Blau, W. J.; Byrne, H. J.; Muster, J.; Burghard, M.; Roth, S. *Chem. Phys. Lett.* **1999**, *310*, 8.
(29) Hartschuh, A.; Sanchez, E. J.; Xie, X. S.; Novotny, L. *Phys. Rev. Lett.* **2003**, *90*, 095503.
(30) Hayazawa, N.; Yano, T.; Watanabe, H.; Inouye, Y.; Kawata, S. *Chem. Phys. Lett.* **2003**, *376*, 174.
(31) Yano, T. A.; Inouye, Y.; Kawata, S. *Nano Lett.* **2006**, *6*, 1269.
(32) Anderson, N.; Hartschuh, A.; Novotny, L. *Nano Lett.* **2007**, *7*, 577.
(33) Yao, Y. G.; Li, Q. W.; Zhang, J.; Liu, R.; Jiao, L. Y.; Zhu, Y. T.; Liu, Z. F. *Nat. Mater.* **2007**, *6*, 283.
(34) Zhang, Y. Y.; Zhang, J.; Son, H. B.; Kong, J.; Liu, Z. F. *J. Am. Chem. Soc.* **2005**, *127*, 17156.
(35) Brown, K. R.; Walter, D. G.; Natan, M. J. *Chem. Mater.* **2000**, *12*, 306.
(36) Duesberg, G. S.; Loa, I.; Burghard, M.; Syassen, K.; Roth, S. *Phys. Rev. Lett.* **2000**, *85*, 5436.
(37) Xu, H. X.; Kall, M. *ChemPhysChem* **2003**, *4*, 1001.
(38) Duan, X. J.; Zhang, J.; Ling, X.; Liu, Z. F. *J. Am. Chem. Soc.* **2005**, *127*, 8268.
(39) Dresselhaus, M. S.; Dresselhaus, G.; Jorio, A.; Souza, A. G.; Saito, R. *Carbon* **2002**, *40*, 2043.
(40) Rao, A. M.; Richter, E.; Bandow, S.; Chase, B.; Eklund, P. C.; Williams, K. A.; Fang, S.; Subbaswamy, K. R.; Menon, M.; Thess, A.; Smalley, R. E.; Dresselhaus, G.; Dresselhaus, M. S. *Science* **1997**, *275*, 187.
(41) Videen, G. *J. Opt. Soc. Am. A* **1991**, *8*, 483.
(42) Assmus, T.; Balasubramanian, K.; Burghard, M.; Kern, K.; Scolari, M.; Fu, N.; Myalitsin, A.; Mews, A. *Appl. Phys. Lett.* **2007**, *90*, 173109.
(43) Kneipp, K.; Jorio, A.; Kneipp, H.; Brown, S. D. M.; Shafer, K.; Motz, J.; Saito, R.; Dresselhaus, G.; Dresselhaus, M. S. *Phys. Rev. B* **2001**, *6308*, 081401.